JOURNAL OF THERMOPHYSICS AND HEAT TRANSFER
Vol. 7, No. 2, April–June 1993

Theory of Radiation from Low Velocity Shock Heated Air

D. A. Levin* and R. T. Loda†
Institute for Defense Analyses, Alexandria, Virginia 22311
G. V. Candler‡
North Carolina State University, Raleigh, North Carolina 27695
and
C. Park§
NASA Ames Research Center, Moffett Field, California 94035

Application of hypersonic computational fluid dynamics models to low velocity vehicles is examined. Important modeling aspects such as chemical kinetics, electronic excitation/de-excitation mechanisms, and existence of equilibrium vs nonequilibrium conditions in the flow were examined. Flowfield properties and in-band radiances in the wavelength region of 0.25 μ in the vicinity of the stagnation streamline are given for a hemisphere with a radius of 0.0762 m. Comparison with recent shock tube data is also shown.

Background and Introduction

A BASIC technological problem that is of importance to the strategic defense initiative is the prediction of radiation levels produced by aerodynamically shock heated air for vehicles moving at speeds and altitudes appropriate to the boost phase scenario. Most of the research to date in radiation emitted from hypersonic flowfields has focused on re-entry conditions at velocities above 7 km/s and nose radii about an order of magnitude larger than is typical of boost phase vehicles. This in turn has also impacted the understanding of the relevant physics required at slower speeds.[1]

In preparation for a rocket experiment sponsored by the Innovative Science and Technology Office of the Strategic Defense Initiative Organization (SDIO) that will measure the in-situ bow shock radiation from a 0.1016-m (4-in.) nose radius vehicle,[2] calculations have been undertaken to predict signal levels at speeds appropriate to selected exit trajectory conditions. These calculations have also served to identify critical regions where the present computational modeling may be questionable. Comparison of shock tube calculations using the STRAP model of Park[3] with shock tube measurements[4] will also be presented here.

Figure 1 shows a comparison of calculated spectra of shock heated air for different speed and altitude conditions relevant to boost phase and re-entry conditions, respectively. The spectra are integrated over temperature and species concentrations from the shock to the body along the stagnation streamline using the NEQAIR (nonequilibrium air radiation) model written by Park.[5] Examination of Fig. 1 shows the following features. The lack of N_2^+ radiation at the slower speed is readily apparent. NO is seen to be the dominant radiator for a shock heated oxygen and nitrogen mixture. Hence, the chemical production and destruction mechanisms of NO are the key ones.

Also, we found for the lower velocity case, that about two orders of magnitude fewer electrons were produced. Their energy is about 0.5 eV, rather than the 2.25 eV that is typical of re-entry conditions. This increases the importance of neutral collisional excitation mechanisms; the adequacy of such modeling at slower speeds in NEQAIR is discussed here as well.

Finally, the importance of a multitemperature model vs a single temperature model in this flight regime was closely examined. The validity of a combined vibrational-electronic temperature at shock conditions even weaker than those that correspond to Fig. 1 is also of concern, but has not yet been resolved. Due to smaller shock stand off distances and nonequilibrium conditions the modeling of relaxation mechanisms among the translational, vibrational, and electron energy modes in the flow is crucial. At altitudes above 40 km and speeds less than 3.5 km/s, temperatures, species concentrations such as NO and O, and UV radiation were found to be significantly different from equilibrium vs nonequilibrium modeling.

This work has borrowed much from a set of computational tools developed by two of the co-authors of this article. The one-dimensional SPRAP/STRAP[3] and NEQAIR[5] codes developed by Park, and a two-dimensional code developed by Candler[6] (coupled with NEQAIR) were used to compute radiation at the stagnation point and about the body. We initially used the SPRAP and NEQAIR codes of Park and later the two-dimensional code of Candler (designated two-dimensional). Flowfield properties predicted by the SPRAP and two-dimensional models such as temperatures, relaxation times, and major species concentrations were compared. At a speed of 4.1 km/s, 40-km altitude, and a nose radius of 0.0762 m, the average temperature $\sqrt{TT_v}$ and relaxation times were essentially equal. At the same conditions the SPRAP code predicted a factor of two, higher in both the amount of NO produced and radiance obtained in the spectral range of 0.225–0.275 μ. Factor of two differences in the flowfield solutions were considered to be adequate agreement and were attributed primarily to the modeling of the shock thickness and inclusion of reacting chemistry in the shock, both of which are incorporated only in the two-dimensional code.[1] The decision to proceed with the two-dimensional code for calculation of bow shock flowfield properties was to enable computation of a two-dimensional radiation map to deduce the radiating area of the stagnation region. Another distinction in the two models that we found to be crucial at speeds lower than 3.5 km/s and altitudes higher than 40 km for nose radii on the order of 0.1 m, is the inclusion of boundary-layer effects. At these conditions for flows with Reynolds numbers Re less than about 70,000, where $Re = \rho_\infty u_\infty r_n/\mu_\infty$, the boundary layer subsumes a significant portion of the flow. The two-

Presented as Paper 90-0133 at the AIAA 28th Aerospace Sciences Meeting, Reno, NV, Jan. 8–11, 1990; received May 17, 1990; revision received Dec. 24, 1990; accepted for publication April 30, 1992.

*Research Staff, Science and Technology Division, 1801 N. Beauregard St. Member AIAA.
†Research Staff, Science and Technology Division, 1801 N. Beauregard St.
‡Assistant Professor, Department of Mechanical Aerospace Engineering. Member AIAA.
§Research Scientist. Associate Fellow AIAA.

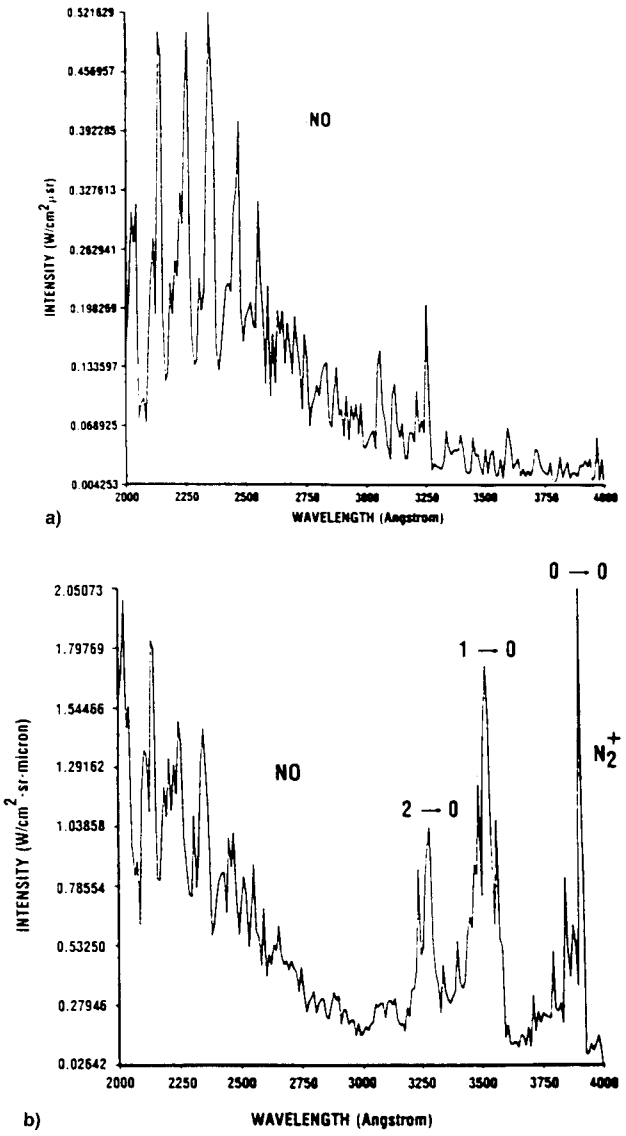

Fig. 1 Comparison of spectra under different shock conditions: a) v = 3.9 km/s, 40-km altitude, 0.1016-m nose radius and averaged over a spectral width of 10 Å; b) v = 7.3 km/s, h = 51.7 km, 0.0762-m nose radius, and averaged over a spectral width of 10 Å. Peak height ratio of 1 → 0 and 0 → 0 is an artifact of the spectral range cutoff at 4000 Å.

dimensional code incorporates such a model, therefore permitting its use at weaker shock conditions.

Kinetic Rate Analyses of the Flowfield Chemical Equation

The above-mentioned models utilize finite-rate chemistry coupled to the flow instead of assuming equilibrium conditions. For the flight regime for which they were originally developed, the chemical reaction time scale is on the order of the convection time scale of the flow. When we began applying these models to boost phase trajectories several questions were raised regarding the adequacy of the chemical kinetics incorporated in the models. We developed a simple kinetics model that allowed us to explore issues such as 1) the degree to which chemical reactions were unequilibrated; 2) sensitivity to rate and equilibria constants; and 3) sensitivity to freestream boundary conditions due to the presence of trace atmospheric species. The chemical kinetic model that we used incorporated the following six reactions:

$$N_2 + M \rightleftarrows 2N + M \quad (1)$$

$$O_2 + M \rightleftarrows 2O + M \quad (2)$$

$$NO + M \rightleftarrows N + O + M \quad (3)$$

$$N_2 + O \rightleftarrows NO + N \quad (4)$$

$$NO + O \rightleftarrows O_2 + N \quad (5)$$

$$N + O \rightleftarrows NO^+ + e^- \quad (6)$$

where M represents a collision partner and includes the seven following species N_2, O_2, NO, N, O, e^-, and NO^+. Tables 1 and 2 provide a list of the forward rate coefficients k_f and equilibria constants K_{eq} used for the six chemical reactions and collision partners specified in Eqs. (1–6) above. The backward rate coefficients are computed from the ratio of the forward rate coefficient to the equilibria constant.[7–9] A system of first-order ordinary differential equations was solved to obtain concentration as a function of reaction time for each of the seven species using standard kinetic rate formalism.[10] Gear's method[11] was employed since the equations are stiff. To analyze our results we used species concentrations at a representative time of 10 μs as a significant measure. An important caveat about the results to be presented is that due to the limited number of chemical reactions modeled, the analysis would not be valid for temperatures higher than 8000 K (that are, e.g., produced at orbital velocities).

Figure 2a shows the change in species mole fraction for N_2, O_2, NO, O, and e^- as a function of reaction time assuming a gas temperature of 5000 K, a gas pressure of 0.01 atm, and 79% N_2, 21%, O_2 initial composition. Figures 2b–g show the rate of change of the same species concentrations. At a reaction time of 100 μs the solutions are still not equilibrated. Basically, the time to reach chemical equilibrium will depend on the pressure (maximum order cubic) and temperature. When the calculation is carried out to reaction times of 10^3 and 10^4 μs [N_2] and [O] were seen to equilibrate. The same calculations were repated at a pressure of 0.5 atm with the result that all species were equilibrated between 10^3–10^4 μs reaction time.

The importance of choosing chemical processes and their respective rate constants consistent with the high temperature flow environment has been examined extensively by Park.[8,12,13] Due to the reinterpretation by Park[12] of the high temperature rate data, the STRAP/SPRAP and two-dimensional flowfield codes do not have the same kinetics data base. The former set of codes uses values given in Ref. 7, whereas the latter code uses values taken from Refs. 8 and 9. Therefore, a comparison of species concentrations obtained at 10 μs with our kinetic model using the two different sets of rate data and equilibria constants, demonstrates the importance of these differences, in our flight regime. The differences in the Park and Candler models are dominated by dissimilar equilibria constants (see Table 2). When the latter set of equilibria constants are used, predictions obtained with either set of rate coefficient data (from Table 1) agree within a factor of two above 4000 K for 40–60 km altitude freestream conditions.

The kinetics results shown so far were generated assuming that initially there is only N_2 and O_2 present. Standard atmospheric models,[14–16] however, show that at 40 km there are trace amounts of O, NO, and O_3 present (about five orders of magnitude lower in concentration). Possible changes in the results of the simulation due to initially nonzero amounts of trace species were examined. Since ozone will be dissociated at a temperature of 1000 K or greater,[17] its principal effect is to increase the atomic oxygen concentration in the freestream. The calculations were repeated with freestream conditions chosen to correspond to the above-referenced atmospheric models. At temperatures of 5000 K and higher, differences of less than a factor of two in species concentrations produced at 10-μs reaction time were observed regardless of the atmospheric model chosen. Comparison of kinetic model results

Table 1 Forward rate coefficient parameters[a]

Reaction[b]	Collision[c] partner	Park[d] C_{ij}^c	Park[d] η_{ij}	Park[d] θ_i^d	Candler[e] C_{ij}	Candler[e] η_{ij}	Candler[e] θ_i
1	N_2	3.7×10^{21}	−1.6	113,200	3.7×10^{21}	−1.6	113,200
	O_2	3.7×10^{21}	−1.6	113,200	3.7×10^{21}	−1.6	113,200
	NO	4.98×10^{21}	−1.6	113,200	4.98×10^{21}	−1.6	113,200
	N	1.60×10^{22}	−1.6	113,200	1.60×10^{22}	−1.6	113,200
	O	4.98×10^{22}	−1.6	113,200	4.98×10^{22}	−1.6	113,200
	e	8.30×10^{24}	−1.6	113,200	8.30×10^{24}	−1.6	113,200
	NO^+	——	−1.6	113,200	3.70×10^{21}	−1.6	113,200
2	N_2	9.68×10^{22}	−2.0	59,750	2.75×10^{19}	−1.0	59,550
	O_2	9.68×10^{22}	−2.0	59,750	2.75×10^{19}	−1.0	59,550
	NO	9.68×10^{22}	−2.0	59,750	2.75×10^{19}	−1.0	59,550
	N	2.90×10^{23}	−2.0	59,750	8.25×10^{19}	−1.0	59,550
	O	2.90×10^{23}	−2.0	59,750	8.25×10^{19}	−1.0	59,550
	e	9.68×10^{22}	−2.0	59,750	1.32×10^{22}	−1.0	59,550
	NO^+	——	−2.0	59,750	2.75×10^{19}	−1.0	59,550
3	N_2	7.95×10^{23}	−2.0	75,500	2.3×10^{17}	−0.5	75,500
	O_2	7.95×10^{23}	−2.0	75,500	2.3×10^{17}	−0.5	75,500
	NO	7.95×10^{23}	−2.0	75,500	2.3×10^{17}	−0.5	75,500
	N	7.95×10^{23}	−2.0	75,500	4.6×10^{17}	−0.5	75,500
	O	7.95×10^{23}	−2.0	75,500	4.6×10^{17}	−0.5	75,500
	e	7.95×10^{23}	−2.0	75,000	7.36×10^{19}	−0.5	75,000
	NO^+	——	−2.0	75,000	2.30×10^{17}	−0.5	75,000
4	——	6.44×10^{17}	−1.0	38,370	3.18×10^{13}	0.10	37,700
5	——	8.37×10^{12}	0.0	19,450	2.16×10^{8}	1.29	19,220
6	——	1.53×10^{9}	0.37	32,000	6.50×10^{11}	0.00	32,000

[a]The forward rate coefficient for the ith chemical reaction and jth species is defined as, $k_f^{ij} = CijT^{\eta ij} \exp(-\theta_i/T)$ units of Cij and θ_i are in cm³/(molecules/s) and K, respectively.
[b]See text equation numbering.
[c]Symbol M discussed in text.
[d]Taken from Ref. 7.
[e]Taken from Refs. 8 and 9.

Table 2 Equilibria reaction constants[a]

Reaction[b]	A_{1m}	A_{2m}	A_{3m}	A_{4m}	A_{5m}
			Park[c]		
1	1.858	−1.325	−9.856	0.174	0.008
2	2.855	0.988	−6.181	0.023	−0.001
3	0.792	−0.492	−6.761	−0.091	0.004
4	1.066	−0.833	−3.095	−0.084	0.004
5	−2.063	−1.480	−0.58	−0.114	0.005
6	−7.053	−0.532	−4.429	0.150	−0.007
			Candler[d]		
1	3.898	−12.611	−0.683	0.118	0.006
2	1.335	−4.127	−0.616	0.093	−0.005
3	1.549	−7.784	−0.228	−0.043	0.002
4	2.349	−4.828	−0.455	−0.075	0.004
5	0.215	−3.652	−0.843	−0.136	0.007
6	−6.234	−5.536	−0.494	0.058	−0.003

[a]The equilibria reaction constants are computed as $K_{eq_m} = \sum_{i=1}^{5} A_{im}[10{,}000/T(\mathrm{K})]^{(i-1)}$ where m indicates the chemical reaction index.
[b]See text equation numbering.
[c]Reference 7.
[d]Reference 10.

obtained with only N_2 and O_2 initially present vs those with trace atmospheric species present showed significant differences. At a temperature of 4000 K or higher, atomic oxygen was found to be the chemistry initiator resulting in about two orders of magnitude more NO formed after 10 μs.

Since the kinetic modeling indicated a sensitivity to atomic oxygen concentration, the full flowfield and radiation calculation were repeated with the freestream mass fraction of O and NO increased from 10^{-12}–10^{-6} at 50-km altitude. At a speed of 3.5 km/s we obtained no difference in the NO gamma-band radiation calculated. At a weaker shock condition of 3.0 km/s a factor of 4 difference was obtained. This is probably due to the effect of lower temperatures and less NO being produced. Thus, the majority of radiation is produced by the NO initially present.

Examination of Radiation Modeling in the Ultraviolet

As Fig. 1 shows, the flowfield and aforementioned radiation model NEQAIR[5,18] predict predominantly NO(γ) band radiation. In our examination of the radiation modeling in the 2500 Å spectral regime, we explored three issues: 1) conditions that produce the maximum radiation; 2) adequacy of a modeled recombinative excitation mechanism, and 3) neutral collisionally induced excitation of NO. Electron excitation/deexcitation mechanisms of NO have been considered elsewhere[5,18] and for our purposes were assumed adequate.

The NO molecule is modeled as a three-level system comprised of the X, A, and B electronic states. The neglect of radiative decay contributions from higher electronic levels is not considered significant due to insufficient energy in the flow to populate such states. Figure 3a shows the flowfield heavy particle translational temperature T and the vibrational temperature T_v along the stagnation streamline for a sphere with 0.0762-m nose radius, an altitude of 40 km, and a speed of 3.5 km/s. The assumption is made that all molecular vibrational models in the flow are characterized by the same vibrational temperature T_v. This should have minimal effect on the flowfield solutions since about 78% of the flow is composed of N_2. The calculated radiative heat density E(W/cm³) is integrated over the NO(γ) bands from 2250 to 2750 Å. E peaks in the region where T and T_v are nearly equilibrated. Using the quasi-steady-state (QSS) approximation the populations of the A and B electronic state are calculated from the flowfield values of T, T_v, and ground state NO generated from the flowfield calculations. Figure 3b compares the ex-

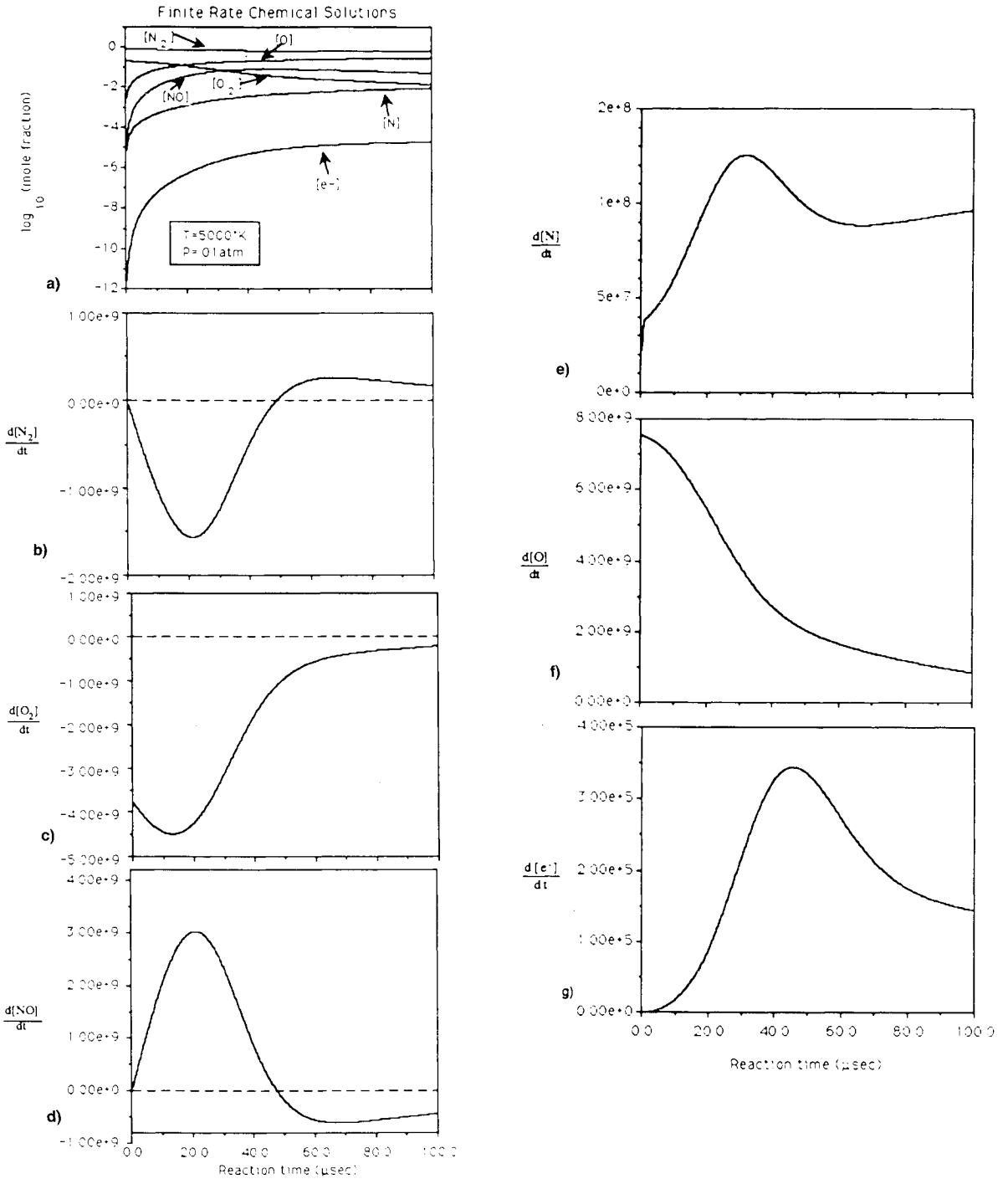

Fig. 2 Finite rate kinetics for a gas temperature of 5000 K, ambient conditions of 40 km, and total reaction time of 100 μs.

cited state populations derived in the QSS approximation with those calculated assuming a Boltzmann distribution at T_v. The QSS derived populations are about 30% lower than those obtained using a Boltzmann distribution.

Since N_2 composes about 78% of the flow, its population distribution is also characteristic of the salient electronic excitation mechanism. Under the same conditions as discussed above, the first three excited state populations [i.e., $A(^3\Sigma_u^+)$, $B(^3\Pi_g)$, and $(^1\Pi_g)$] obtained from a Boltzmann distribution were also found to be about 30% higher than those obtained in the QSS approximation.

Therefore, while it cannot be shown rigorously, it is reasonable to argue that for these gas conditions the Boltzmann population represents the maximum A and B state populations achievable. Any additional changes in specific excitation cross sections will not produce a proportional enhancement in radiation.

The use of the QSS approximation is found to be valid as well. The QSS approximation assumes a zero net rate of change of population from an electronic state. This approximation is valid when there are a sufficient number of collisions in the flow relative to the shortest radiative lifetimes of interest. The decoupling of the electronic excitation/de-excitation calculations from the flowfield solutions further assumes that the former processes are fast relative to convection flow time scales. The first criterion is satisfied since the QSS predicted excited state populations approach a Boltzmann distribution. The second criterion is also satisfied since the radiative lifetime of the NO(A) state is about 0.2 μs compared with 10 μs time scales representative of the flow.

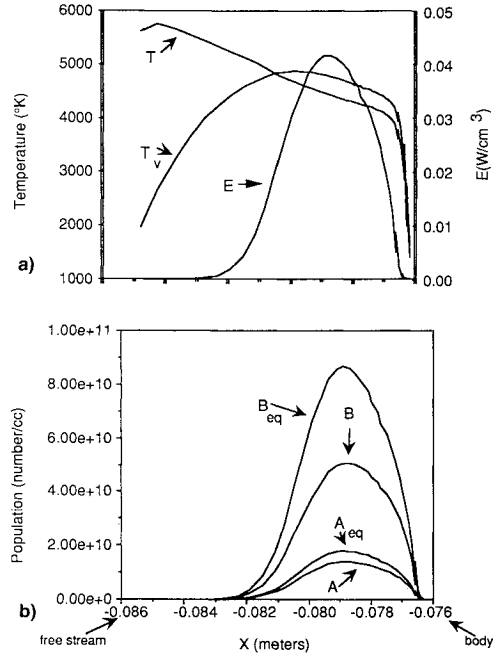

Fig. 3 Baseline comparison of QSS vs equilibrium population distributions for different locations along stagnation streamline: a) comparison of heavy particle temperature T, vibrational temperature T_v, and radiance E; b) comparison of A and B state populations in the QSS vs Boltzmann models.

An important mechanism for populating excited states of NO is three body recombination

$$N + O + (M) \rightarrow NO^* + (M) \tag{7}$$

where (M) represents a third body such as N_2, and NO^* denotes an excited state of that molecule. NEQAIR does not explicitly model multiple species intermolecular electronic state coupling. Thus, the comparison we will make with shock tube data utilizes the approximation that the details of the total mechanism are dominated by the potential energy barrier of the NO excited states. The population of the C state is ignored since T_v is on the order of 5000 K. The specific rate data that are programmed in NEQAIR were taken from Ref. 19. Alternative rates were proposed by Gross and Cohen[20] from their experiments in a glow discharge shock tube. They assessed their rates to be valid over a temperature range of 300–2000 K. Under the conditions of their experiment, NO gamma (A) and beta (B) band radiation was measured. Excited and ground dissociation rates can be inferred from these measurements. The rate of formation of NO in the ground state and production of a gamma band photon proceeding through the A state is

$$N + O + (N_2) \rightarrow NO + (N_2) + h\nu(\gamma) \tag{8a}$$

where all species are in the ground state and

$$\frac{d[NO]_i}{dt} = \left\{10^{-16.9}\left(\frac{300}{T}\right)^{0.35} + 10^{-33.8}\left(\frac{300}{T}\right)^{1.24}[N_2]\right\}[N_2][O]\ \frac{\text{particles}}{\text{cm}^3\text{s}} \tag{8b}$$

where i denotes either the X or A state. The term $h\nu(\gamma)$ in Eq. (8a) denotes a gamma band photon emitted. The square brackets in Eq. (8b) specify concentration of the enclosed species, here in particles/cm^3. Determination of the population of the B state from measurement of beta-band radiation is not as straightforward. The presence of other closely lying electronic states complicates the analysis. A factor of 35 can be attributed specifically to the B state.[20] Thus

$$\frac{d[NO]_i}{dt} = \frac{1}{35} \times 10^{-33.52}\left(\frac{T}{300}\right)^{1.4}[N][O][N_2] \tag{8c}$$

in particles/cm^{3}s and the subscript i denotes the B state. To compare with NEQAIR (where the reverse rate—a dissociation rate, is given) Eqs. (8b) and (8c) must be multiplied by the respective equilibria constants.

The dissociation rate coefficient used in NEQAIR is of the form

$$k_{\text{dissoc}} = \chi_{\text{atom}}(0.0184) + \chi_{\text{molec}}(4.56 \times 10^{-7})T^{-1.6} \cdot \exp[-(D_e - T_e)/kT] \tag{8d}$$

where χ_{atom} and χ_{molec} are the fraction of atomic and molecular species in the flow, and D_e and T_e are the dissociation limit and term value of the excited state level, respectively. The specific numerical coefficients given in Eq. (8d) are specific to NO and are independent of electronic level.

Table 3 gives a summary of the calculations and a direct comparison for the two sets of dissociation rates. The molecular parameters taken for D_e and T_e conform to those given in potential energy calculations of Gilmore.[21] The first conclusion one can draw is that the rate presently given in NEQAIR for the A state discussion is actually almost an order of magnitude less than that given by Gross and Cohen. Therefore, the value used in NEQAIR would tend to predict slightly more radiation rather than that of Gross and Cohen, since population is being lost less readily from the A state through dissociation. Table 3 also shows that there is a larger difference in the B state dissociation predicted by Gross and Cohen vs Park. Also there is a reversal in the relative sizes. Examination of Eq. (8d) and the footnotes of Table 3 shows that two A and B state rates of Park are explicitly related to each other by a factor of $\exp[-(D_{eA} - D_{eB})/kT]$ or 0.5475 at T = 4700 K. If the Gross and Cohen values were assumed correct and the B state value was adopted, this would also tend to decrease the amount of gamma band radiation through the coupling of the three electronic states. The absolute magnitude, however, of the decreased radiation would be less due to the lower transition probability of radiation from the B vs A state to the ground state.

Finally, collisional excitation of NO is another important source of NO(A)

$$N_2(A) + NO(X) \rightarrow N_2(X) + NO(A) \tag{9a}$$

or in rate form

$$\frac{dn_i}{dt} = K_{fi}^{n1} n_1 n_j \tag{9b}$$

where K_{fi}^{n1} is the rate coefficient and n_i, n_j, and n_1 represent the concentration of NO(A), NO(X), and $N_2(A)$, respec-

Table 3 Tabulation of comparison between collisional dissociation rates of NO in NEQAIR and Gross and Cohen[a]

T = 4700 K, χ_{atom} @ 0.1, χ_{molec} @ 0.9		
Equilibrium constant	Gross & Cohen K_{dissoc}	Park K_{dissoc}
A State		
7.10×10^{23}	4.89×10^{-12}	5.0×10^{-13} [b]
B State		
1.49×10^{23}	2.74×10^{-14}	9.1×10^{-13} [c]

[a]All units are in molecules/cm^3.
[b]D_e, T_e used were 71, 718, and 43,965 cm^{-1}, respectively.
[c]D_e, T_e used were 71, 718, and 45,933 cm^{-1}, respectively.

tively. The corresponding process is indirectly modeled in NEQAIR. n_1 represents the total neutral molecular density and is not molecule or electronic state specific. The rate coefficient is modeled in the form of a generalized ramp cross section

$$K_{ij}^{n_1} = 4057kT^{1/2}\sigma e^{-x}\left(\frac{x^2 + 2.334733x + 0.250261}{x^2 + 3.330657x + 1.681534}\right) \tag{10a}$$

where

$$x \equiv \frac{T_e^u - T_e^l}{kT} \tag{10b}$$

and T_e^u and T_e^l are the energy term values for the upper and lower electronic states, and T is the heavy particle temperature. The present value used for σ is 1.0×10^{-16} cm^2 and is the same for all molecular systems. For NO, however, other experiments indicate that such a collisional excitation process is more efficient; i.e., σ may be about a factor of ten higher. The rate coefficient obtained from an experiment by Piper and co-workers[22] was normalized to match the flow concentrations of NO(X), NO(A), $N_2(X)$, and $N_2(A)$ predicted by NEQAIR and then compared with Eqs. (9b) and Eqs. (10a) and (10b) to give a σ that corresponds to 9.0×10^{-16} cm^2.

In summary, differences were found between selected rate coefficients presently programmed in NEQAIR and values suggested by the above-referenced literature. The net result, however, of these discrepancies is to predict NO molecular in-band radiances similar to the baseline version of the model.

Shock Tube Radiance Calculations and Comparison with Experiment

Using STRAP and NEQAIR, we obtained model predictions with new shock tube data taken under 3.2–3.8-km/s and 40–55-km conditions.[3] The filter function used in NEQAIR to calculate the in-band radiance corresponding to the experiment was of the form

$$T = T_0 \exp[-(\lambda - \mu_0)^2/2\sigma^2] \tag{11}$$

where $T_0 = 0.15$, $\mu_0 = 2590$ Å, and $\sigma = 42.466$ Å.

The field of view of the radiometer was accounted for by use of a Gaussian spreading function[3] in STRAP. An intermediate value of 0.4 cm was chosen to correspond with the quoted[3] value of 0.3–0.5-cm spatial extent. The domain over which STRAP computes the viscous calculation χ_ρ was varied. Comparison of the final radiation showed no sensitivity to the χ_ρ parameter.

Figure 4 shows a comparison of the peak radiation values obtained from theory and experiment. Radiance was found to scale with altitude and velocity for both theory and experiment. Bow shock radiance results given in the next section, however, show a very different scaling behavior. The reason for this different scaling behavior is not fully understood, however, shock tube simulations may provide some indications. Examination of the lower Reynolds number shock tube simulations showed that the location of the radiance peak moves further from the shock. Therefore, in the presence of a cool wall the peak radiation may be suppressed and may not produce a scaling relationship similar to that obtained with the shock tube results.

In addition to comparing the absolute magnitude of radiation, we also verified the general spatial profile of radiation predicted by theory. The actual radiance profile as a function of location from the shock front is a complicated function of chemical kinetics, energy exchange relaxation, and excitation/de-excitation processes. Subsequently, comparison of theory and experiment in this case cannot provide in-depth validation of the modeling, but provides qualitative assessment. To compare radiation profiles we needed to transform from time in the laboratory reference frame to distance in the reference frame of the shock (which is what is used in the calculations). Measured radiance vs time[3] for a shock condition of 3.81 km/s at 40-km altitude was digitized and converted to distance from the start of the shock by multiplying the abscissa by the known shock velocity. In Fig. 5 the experimental data (dashed line), the unspread theory (infinitesimal field of view, solid line), and the spread theory (dashed line) are shown. The relative origins along the abscissa for the three curves are arbitrary and have been shifted for comparison. The actual magnitude of the shift is determined by the radiometer window placement in the shock tube. The unspread theory and experimental peak radiances vary by a factor of four, whereas when the spreading function is used the theoretical peak radiance is in agreement with experiment within a factor of two. This is the correct trend since account for the field of view effectively renormalizes and lowers the in-band radiance. The width of the peaks are in qualitative agreement with the experimental peak, but appear to be slightly broader. Given experimental un-

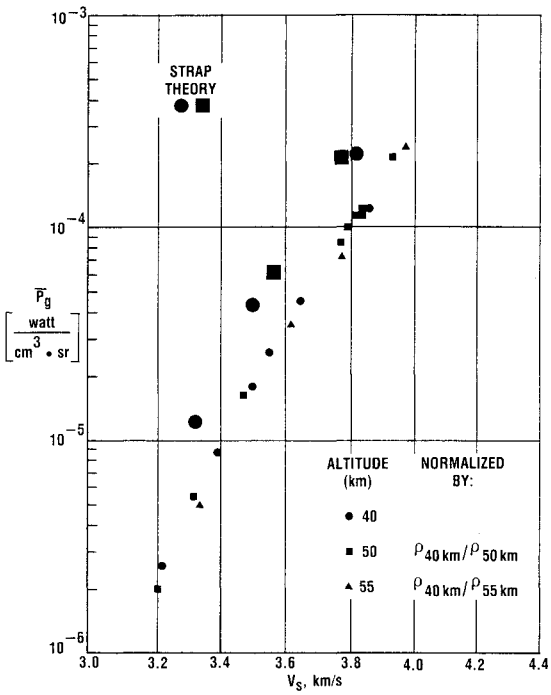

Fig. 4 Comparison of shock tube experimental (CALSPAN) and model (present) results. Data are indicated by smaller symbols.

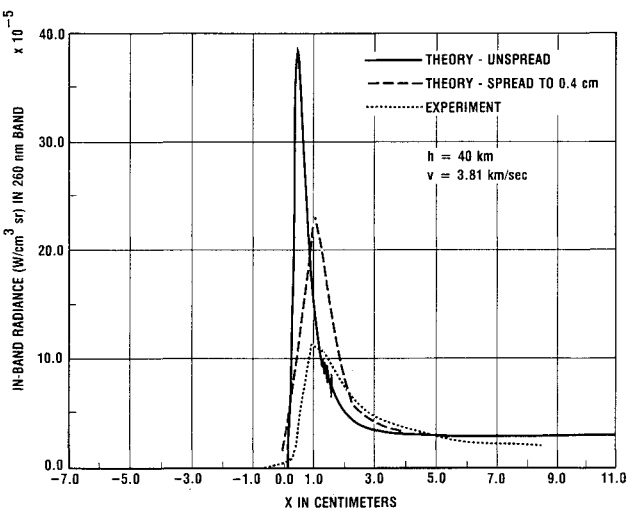

Fig. 5 Finite field of view factor and transformation from laboratory reference frame.

certainties such as the actual location of the shock front and the instrument field of view, more detailed modeling and comparison of the radiation profile was not investigated.

Departure from Equilibrium

The results summarized in this section have been used in the early instrumentation planning stages of an upcoming sounding rocket experiment, as well as to illustrate the relevance of nonequilibrium modeling at the velocities discussed here. The degree of thermal nonequilibrium (i.e., more than a single temperature is required) can be assessed by comparisons of the flowfield solutions generated by single and multiple temperature versions of the model. This also serves to provide a theoretical upper limit to the amount of radiation within the framework of the present model vis-à-vis chemistry and transport. Uncertainties in vibrational-translational energy transfer mechanisms are eliminated in a one temperature model, although, such a model is not physically correct.

A detailed comparison of flowfield state variables such as translational temperature and NO and O concentrations, was made for a 3.7 km/s, 60-km altitude case where (as shown in Fig. 6) there is a difference of about three orders of magnitude in the radiance for the multiple vs single-temperature model. The multiple-temperature model assumes two distinct temperatures, T and T_v. Many of the chemical kinetic rate constants are assumed to be a function of an average temperature that is defined to be $\sqrt{TT_v}$. The single-temperature model solves the same set of conservation equations as is solved in the multi-T model with T set equal to T_v. Two factors account for the lower radiance value obtained with the multitemperature model. As expected, that model gives lower values for T_v than the single-temperature model. Also, since the concentration of radiating species is dependent upon chemical rates that use a lower value of $\sqrt{TT_v}$ instead of T, almost an order of magnitude less NO is produced than for the single-temperature model. Evidence of less reactive chemistry is also observed for atomic oxygen as well. Figure 6 shows a summary of radiance levels as a function of velocity for 40, 50, and 60 km, and for the multiple and single-temperature models along the stagnation streamline. Comparison of the multiple vs single-temperature model results shows that at higher velocities and lower altitudes the two models tend to merge. In both limits there are a greater number of collisions in the flow which leads to equilibrium. By 50 km, however, and 3.5 km/s, there is about an order of magnitude discrepancy with the single-temperature model over-predicting the amount of radiation produced. At 60 km the single-temperature model would overestimate the radiance by many orders of magnitude. In fact, the 60-km multi-temperature result is also probably optimistically high due to combination of the electronic-vibrational temperature assumed here. As discussed in Ref. 2, the optical instruments for a rocket experiment have been designed to provide answers to this very question.

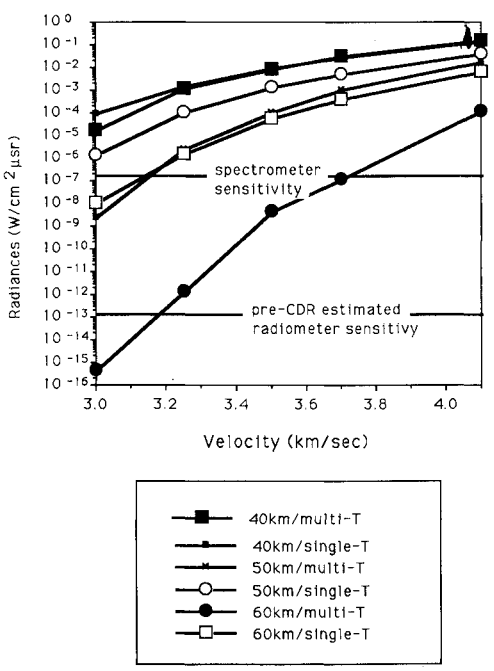

Fig. 6 Summary of 0.0762-m nose radius radiances.

Conclusions

The work discussed here has shown that computational tools developed for a different flight regime can be extended to weaker shocks produced by vehicles with smaller nose radii, moving at slower speeds.

Examination of the kinetics as presently incorporated in the models shows the continued need for full finite-rate chemistry. Differences in rate constants that exist in the literature do not appear to cause large differences in a purely kinetic analysis, and are therefore unlikely to be important in the flow modeling.

The de-excitation/excitation modeling in NEQAIR is valid for shock layer gas conditions formed at 40 km and 3.5 km/s. Nevertheless, the continued use of the QSS approximation to estimate radiation at 0.25 μ becomes questionable by about 60 km due to the fewer number of collisions relative to the lifetime of the NO(A) state. The NEQAIR code has been designed to model excitation processes for a mixture that approaches a Boltzmann limit. At weaker shock conditions there will not continue to be a single mechanism that dominates. Many of the possible intermolecular couplings could become important. The factor of two agreement between shock tube data and modeling supports in a global sense aspects of the modeling related to relaxation and excitation/de-excitation mechanisms. The shock tube results which exist at conditions corresponding to altitudes of up to 55 km and down to speeds of 3.2 km/s produce radiation at 230 nm which scales with density and speed. In contrast, the bow shock radiation values do not scale; the effect of a cool wall boundary condition appears to exponentially extinguish the stagnation region radiation.

Use of the 2-D/NEQAIR model to predict NO(γ) radiation for a 0.0762 m hemisphere as a function of speed and altitude gave interesting trends. As speed and freestream density are reduced, the single-temperature model predicts higher gas radiances then the multitemperature model by many orders of magnitude.

Acknowledgments

This research is supported by SDIO/IST managed by the Army Research Office under Contract MDA903-89-C-0003. We acknowledge the Computational Chemistry Branch of NASA Ames Research Center for providing supercomputer time.

References

[1]Levin, D. A., Loda, R. T., and Collins, R. J., "Theory and Instrumentation Design Considerations for the Measurement of Radiation from Shock Heated Air," Inst. for Defense Analyses P-2207 (to be published).

[2]Levin, D. A. Collins, R. J., and Candler, G. V., "Considerations for the Measurement of Radiation from Low Velocity Shock Heated Air," AIAA Paper 90-0132, Jan. 1990.

[3]Park, C., "Assessment of Two-Temperature Kinetic Model for Ionizing Air," AIAA Paper 87-1574.

[4]Wurster, W. H., Treanor, C., and Williams, M., "Non-Equilibrium UV Radiation and Kinetics Behind Shock Waves in Air," AIAA Paper 89-1981, 1981.

[5]Park, C., "Calculation of Non-Equilibrium Radiation in the Flight Regimes of Aero-Assisted Orbital Transfer Vehicles," *Thermal Design of Aero-Assisted Orbital Transfer Vehicles*, edited by H. F. Nelson, Vol. 96, Progress in Astronautics and Aeronautics, AIAA, New York, 1985.

[6]Candler, G., and MacCormack, R., "The Computation of Hy-

personic Ionized Flows in Chemical and Thermal Non-Equilibrium," AIAA Paper 88-0511, 1988.

[7]Park, C., "Assessment of Two-Temperature Kinetic Model for Ionizing Air," AIAA Paper 87-1574, 1987.

[8]Park, C., "On Convergence of Computation of Chemically Reacting Flows," AIAA Paper 85-0247, Jan. 1985.

[9]Bussing, T. R., and Eberhardt, S., "Chemistry Associated with Hypersonic Vehicles," AIAA Paper 87-1292, 1987.

[10]Candler, G. V., "The Computation of Weakly Ionized Hypersonic Flows in Thermo-Chemical Nonequilibrium," Ph.D. Dissertation, Stanford Univ., Stanford, CA, June 1988.

[11]IMSL, Inc., MATH/LIBRARY, Vol. 2, Version 1.0, April 1987, pp. 640.

[12]Park, C., Problems of Rate Chemistry in the Flight Regimes of Aero-Assisted Orbital Transfer Vehicles," AIAA Paper 84-1730, June 1984.

[13]Park, C., "Two-Temperature Interpretation of Dissociation Rate Date for N_2 and O_2," AIAA Paper 88-0458, Jan. 1988.

[14]Bauer, E., "The Structure of the Earth's Atmosphere-Lecture Notes," Inst. for Defense Analyses, P-811, Alexandria, VA.

[15]Bortner, M., and Kummler, R., "The Chemical Kinetics and the Composition of the Earth's Atmosphere," General Electric Co., GE-9500-ESC-SR-1, July 24, 1968.

[16]"Suggested Natural Variations in Atmospheric Minor Neutral Species," General Electric Co., CR ARBRL-CR-00375, July 1978.

[17]Kee, R. J., Rupley, F. M., and Miller, J. A., "The Chemkin Thermodynamic Data Base," Sandia Rept. SAND 87-8215. UC-4, April 1987.

[18]Park, C., *Nonequilibrium Hypersonic Aerothermodynamics*, Wiley, New York, 1990.

[19]Park, C., and Menees, "Odd Nitrogen Production by Meteoroids," *Journal of Geophysical Research*, Vol. 83, No. 8, 1978, pp. 4029.

[20]Gross, R., and Cohen, N., "Temperature Dependence of Chemiluminescent Reactions. II. Nitric Oxide After Glow," *Journal of Chemical Physics*, Vol. 48, 1968, p. 2582.

[21]Gilmore, F. R., "Potential Energy Curves for N_2, NO, O_2 and corresponding Ions," *Journal of Quantitative Spectroscopy & Radiative Transfer*, Vol. 5, 1965, pp. 369.

[22]Piper, L. G., Cowles, L. M., and Rawlins, W. T., "State-to-State Excitation of NO($A\,^2\Sigma^+$, $v' = 0, 1, 2$) by $N_2(A\,^3\Sigma_u^+$, $v' = 0, 1, 2$)," *Journal of Chemical Physics*, Vol. 85, 1986, p. 3369.